Soliton locking phenomenon over finite magnetic field region in the monoaxial chiral magnet $CrNb_3S_6$

M. Ohkuma[1],* M. Mito[1,2], Y. Kousaka[2,3], T. Tajiri[4], J. Akimitsu[5], J. Kishine[2,6,7], and K. Inoue[2,8,9]
[1]*Graduate School of Engineering, Kyushu Institute of Technology, Kitakyushu 804-8550, Japan*
[2]*Chirality Research Center, Hiroshima University, Higashihiroshima 739-8526, Japan*
[3]*Department of Physics and Electronics, Osaka Prefecture University, 1-1 Gakuencho, Sakai, Osaka 599-8531, Japan*
[4]*Faculty of Science, Fukuoka University, Fukuoka 814-0180, Japan*
[5]*Research Institute for Interdisciplinary Science, Okayama University, Okayama 700-8530, Japan*
[6]*Division of Natural and Environmental Sciences, The Open University of Japan, Chiba 261-8586, Japan*
[7]*Institute for Molecular Science, 38 Nishigo-Naka, Myodaiji, Okazaki, 444-8585, Japan*
[8]*Graduate School of Science, Hiroshima University, Higashihiroshima 739-8526, Japan and*
[9]*Institute for Advanced Materials Research, Hiroshima University, Higashihiroshima 739-8526, Japan*
(Dated: November 2, 2020)

Previous magnetic measurements for the chiral magnet $CrNb_3S_6$ have shown that the soliton-penetration and soliton-dissipation in the chiral soliton lattice state strongly depend on the crystal size and shape. We performed magnetic measurements for a thin single crystal of $CrNb_3S_6$ with 3 μm thickness, permitting the existence of approximately sixty solitons, and observed the magnetization (M) – magnetic field (H) curve with a remarkable full M-H loop. By investigating the minor loop of the M-H curve in detail, we found that the inside of the full M-H loop allows an infinite number of quasi-stable states for each eigen number of solitons, utilizing a non-negligible distribution of the thickness around 3 μm. This study reveals that in a micro crystal with a chiral axis length of a few micrometers, any magnetic state with an arbitrary soliton number can be created in a certain H range within the full M-H loop.

PACS numbers:

The Dzyaloshinskii-Moriya (D-M) interaction arises from a combined second-order perturbation of the spin-orbit coupling and exchange interaction [1, 2]. The competition of D-M interaction and exchange interaction stabilizes a helimagnetic (HM) state. Through the application of a magnetic field (H) to helimagnets, topological objects such as kinks and vortices can be created [3–7]. In a monoaxial D-M vector system, H applied perpendicularly to the chiral axis creates kinks composed with 2π spin rotation in a ferromagnetic alignment [8]. An ideal kink with uniform spin rotation has zero net moment. Theory predicts that the kinks are located at equal intervals, and they satisfy the sine-Gordon equation, which is a soliton equation [8–10]. Thus, we call the kink a soliton, and the magnetic superlattice is called the chiral soliton lattice (CSL). When H increases from zero, the HM state is transformed into the forced-ferromagnetic (FFM) state via the CSL state, as seen in Fig. 1(a). This transformation is physically understood with the change in soliton number (N) from the maximum permitted for the length of the chiral axis to zero. The recent theoretical studies have shown us how the solitons dissipate (annihilate) and penetrate (nucleate) via the surface [11, 12]. Similarly to other chiral magnets, the nucleation of topological objects must overcome the surface barrier [13–16]. Herein, it is stressed that the change in N must accompany both the dissipation of a soliton across the surface and the subsequent rearrangement of the other solitons in the same interval. In the process of decreasing H, the opposite phenomenon occurs. The question of whether or not the above magnetizing and demagnetizing processes are reversible is an important subject.

A typical monoaxial chiral magnet $CrNb_3S_6$ has a structure in which magnetic Cr^{3+} ion is intercalated between the NbS_2 layers stacked in the direction of c-axis. Below the magnetic ordering temperature (T_c), the HM alignment with the period of 48 nm is stabilized [3, 17]. The propagation vector is along the c-axis and perpendicular to the ab-plane, which is magnetic easy plane. The single crystals usually exhibit the smallest thickness along the helical c-axis (termed type I) [17, 18]. The magnetization (M) measurements as a function of H were conducted for bulk, submillimeter, and micrometer sized crystals [11, 17–23]. It was investigated that how crystal shapes as well as crystal sizes influence both soliton dissipation and penetration. The discrete changes in M in the H-decreasing process are more prominent and occur in a reproducible manner with a smaller crystal size along c-axis (L_c) [20, 21]. The hysteresis area was increased with a decrease in both L_c and area of ab-plane (S_{ab}) [23].

Further in $CrNb_3S_6$, soliton-locking phenomenon was observed inside the hysteresis loop on micrometer sized crystal by XMCD experiment [11]. The XMCD experiments have been conducted for micro crystals with L_c = 10-15 μm and thickness of 0.1 μm. M for the region of 5 μm diameter was observed, and this crystal shape is termed type Ⅱ. The H region for reversible change in N was separated from the irreversible H region. However, XMCD using a large facility is not a commonly performed

experiment. In addition, M of the surrounding area was not observed. Indeed, we also want information on the edge region for crystals with different shapes. If we observe M for the entire crystal, the behavior in the edge region will also be understood.

Based on the aforementioned studies, we obtained physical knowledge regarding the solitons in chiral magnets. The change in N in the H-increasing process can accompany the continuous tilting of the spins constituting solitons along the H direction before their annihilation, so that the discrete change in M is small. On the other hand, in the H-decreasing process, solitons penetrate suddenly from the surface after overcoming the surface activation energy, resulting in the discrete change in M. The soliton-locking phenomenon in the hysteresis loop observed for micro crystals with $L_c < 5$ μm remains a phenomenon to be studied for application in more detail.

We previously reported that M-H hysteresis was enlarged with reduction of L_c in the experiment for crystal with sufficient volume by the superconducting quantum interference devise (SQUID) magnetometer [20, 21, 23] There we learned that M-H hysteresis decreases in the manner proportional to log L_c [23]. Even the crystal with $L_c = 10$ μm does not present prominent M-H hysteresis enough to study the soliton-locking phenomenon. In this study, we reduced L_c down to approximately 3 μm (permitting approximately 63 solitons) using a focused ion beam (FIB) technique, keeping enough S_{ab} to maintain sufficient crystal volume (red star in Fig. 1(b)). We enlarged the M-H hysteresis 6 times larger than that of bulk crystal. By measuring M in the SQUID magnetometer, we obtained extensive information in the M-H curve for the entire thin crystal with sufficient accuracy. Herein, the important factor is to prepare a small type I crystal with large M-H hysteresis. We aim to verify that the soliton-locking originates in the intrinsic nature of CSL. By comparing the results for the crystal with L_c $\sim$ 3 μm and those of micro crystal for XMCD experiments, we can specify the H region where soliton-locking occurs.

A single crystal of $CrNb_3S_6$ was synthesized according to the procedure described in the literature [18]. As the first step, the L_c of bulk single crystal was slowly reduced to 10 μm with precise mechanical polishing [23]. As the second step, L_c was carefully reduced to approximately 3 μm by using the FIB method, as shown in Fig. 2(a). The average surface roughness was evaluated to be $\pm$0.3 μm (see Supplemental material [24]). Consequently, the thin crystal seen in Fig. 1(b) was obtained.

M as a function of H was measured at 5 K much lower than T_c from the paramagnetic state to HM state, using the SQUID magnetometer. The T_c was evaluated to be 127 K by the AC magnetic measurements in the AC field with the frequency of 10 Hz and amplitude of 3.9 Oe, as shown in Fig. 2(b). In all measurements, the H

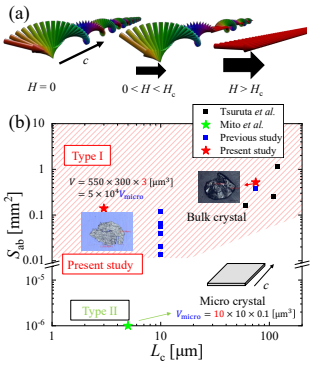

FIG. 1: (Color online) (a) Schematic illustration of the magnetic structure formed in a monoaxial chiral magnet. A helimagnetic state (HM) at zero magnetic field, a chiral soliton lattice (CSL) in the presence of H perpendicular to the helical c-axis, and a forced-ferromagnetic (FFM) state above a critical field H_c. (b) Overview of a series of M measurements for $CrNb_3S_6$ mapping using the c-axis length L_c and the ab-plane area S_{ab} [11, 20, 21, 23]. Optical micrographs of the crystals were taken along the c-axis. There are two approaches: (I) the smallest thickness is along the c-axis (red stripe region) and (II) the c-axis is located on the ab-plane. The shapes are drawn for both the specimens of $L_c \sim 3$ μm and $S_{ab} = 550 \times 300$ μm^2 belonging to (I), and the XMCD specimens with L_c = 10-15 μm and the thickness of 0.1 μm belonging to (II).

and AC field were perpendicularly to the c-axis. The direction of the H might be indeed tilted by few degrees from the perpendicular to the c-axis. According to the reference [25, 26], if the tilting would be more than 2 degree, CSL transforms to tilted CSL that exhibits the soliton annihilation and soliton nucleation. Furthermore, the c-axis is the magnetic hard axis. Indeed, the contribution of conical magnetic structure did not appear in the present experiment. Thus, the effect of the crystal tilting against H is considered to be quite small. The M-H curves shown in this study adopted the averaged value of three M data measured after stabilizing each H. The above T_c value is consistent with those reported in previous studies [20–23, 27, 28], suggesting that the crystal quality related with the exchange interaction is not reduced and the structural disorder discussed in the reference [29] does not occur.

Figure 2(c) shows the full M-H loop at 5 K, which traces the H region of $0 \rightarrow 1.2 \rightarrow 0$ kOe. The critical magnetic field to FFM (H_c), above which there is no hysteresis, is reduced from 2.5 kOe for $L_c \geq 60$ μm or 1.3 kOe for $L_c = 10$ μm [23] to 0.85 kOe via the aforementioned processing. The saturation magnetization (M_s) was approximately 8.0×10^{-5} emu. The shape of the full M-H loop is closer to that in the flat micro crystal of the pre-

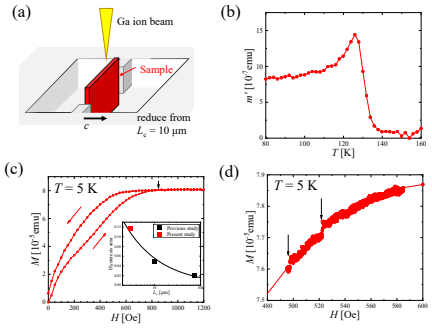

FIG. 2: (Color online) (a) Overview of manufacturing process for micro crystal with $L_c \sim 3$ μm and large S_{ab}. (b) Temperature (T) dependence of real part of AC susceptibility (m') for single crystal of $CrNb_3S_6$ after being processed. (c) M-H for single crystal of $CrNb_3S_6$ after being processed. The inset shows the hysteresis area calculated from M/M_s as a function of H/H_c [23]. The black curve in the inset is a guide for the eyes. (d) Discrete changes of M-H for micro crystal with $L_c \sim 3$ μm after being processed.

vious XMCD experiment (type Ⅱ) [11] rather than that in bulk crystals of type I [20, 21, 23]. For reference, the hysteresis area was smaller with increasing temperature, then disappeared at 130 K, just above the T_c. This indicates that the hysteresis in the M-H curve does not originate from ferromagnetic impurities attached to the $CrNb_3S_6$ crystal.

Figure 2(d) shows the enlarged M-H curve in the H decreasing process below 600 Oe. The discrete change at 525 Oe in the first soliton nucleation was observed . Since the permitted N is approximately 60 in the present crystal with $L_c \sim 3$ μm, the change in M for $\Delta N = 1$ should be 1.3×10^{-6} emu. The first discrete change in M at 525 Oe was 0.3×10^{-6}, which is equivalent with the $\Delta N = 1$ nucleation in the one-fourth area of the crystal. However, the present crystal with $L_c = 3$ μm does not exhibit the large discrete change in M. We suppose that a lot of minute discrete changes occur irregularly due to large distribution of L_c. Thus, we could enlarging hysteresis in the full loop enough to study the minor loop in detail.

Figure 3(a) shows the results for many single return minor loops (SR-ML) at $T = 5$ K in addition to that for the full loop ($0 \rightarrow > H_c \rightarrow 0$); every 50 Oe for $H \leq 250$ Oe, every 10 Oe for $300 \leq H \leq 400$ Oe, and every 25 Oe for $400 \leq H \leq 800$ Oe. Herein, in the full loop curve, the H-increase and H-decrease processes are termed process A and process B, respectively. The process A is divided into two processes, A1 below 280 Oe and A2 above 280 Oe. In our previous study for the crystal with $L_c = 10$ μm, both the experimental and theoretical results suggest that the decrease in the DM interaction at the surface brings about the ferromagnetic alignment at small H [23]. Afterward, in the intermediate region between both edges, the solitons begin to annihilate toward the outside. We now return to discussion of the results for the crystal with $L_c = 3$ μm. As seen in fig. 3(a), the curvature of M-H curve changed at around 300 Oe. In the low H region of $0 < H \leq 280$ Oe, a slight H induces ferromagnetic alignment at the surfaces. The M at 280 Oe was approximately a half of the M_s, such that we assumed that approximately a half of solitons changed the spin texture from helimagnetic to ferromagnetic alignments. Thus, there remained approximately thirty solitons in the intermediate region between the FFM arrays stabilized at both edges. The minor loop within process A1 is considered to be due to the enlargement and reduction of the FFM alignment at both surfaces. In process A2, the soliton number of the helical chain apart from both edges varies as a function of H. When H returns at a certain H (H_r), coinciding with process B, M varies with curvature similar to that of A1. As we shall see later, the process from H_r to a H point on process B shows the reversible changes, such that it is considered to maintain a soliton number. It shows that the inside of the full loop after annihilation of the solitons at both edges is a special region, in which N is locked at a value between 0 and 30. Assuming that the solitons successively annihilate from 300 Oe to H_c with the same H interval, the annihilation of the solitons occurs at intervals of 20 Oe and the H return for every value over 20 Oe should be meaningful. It is possible to change H by increments of 0.15 Oe (the minimum value permitted by the apparatus), such that we can prepare approximately 4000 SR-MLs [(850-280)/0.15 = 3800]. It means that the inside of a full M-H loop allows an infinite number of quasi-stable states with each eigen number of solitons.

Figure 3(b) shows the H dependence of M for three runs starting from process A2, first run of $0 \rightarrow 300$ (A2) $\rightarrow 180 \rightarrow 300$ (A2) $\rightarrow 140 \rightarrow 300$ and second run of $0 \rightarrow 300$ (A2) $\rightarrow 180 \rightarrow 300$ (A2). In the second run, we waited 5 minutes after the H stabilized before measuring M, so that we could obtain the data with less error than that in the first run. All three double-return M loops (DR-ML) were magnetized at $H = 300$ Oe, which is located on process A2. In the demagnetizing process down to a certain point in the hysteresis of the full loop, there is a reversible change in M against the minor loop of $300 \rightarrow 180 \rightarrow 300$, suggesting the locking of N. The minor loop experiencing the reduction of H down to the H points (140 Oe) shows an irreversible change in M.

Figure 3(c) shows the H dependence of M in the run starting from process B, 1200 ($> H_c$) $\rightarrow 200$ (B) $\rightarrow 300 \rightarrow 200$ (B) $\rightarrow 400 \rightarrow 200$ Oe. In the process of 1200 $\rightarrow$200 (B) $\rightarrow 300 \rightarrow 200$ (B), no hysteresis appears. The subsequent process of 200 (B) $\rightarrow 400$ (A2) $\rightarrow 200$ (B) exhibits prominent hysteresis due to the reappeared change in

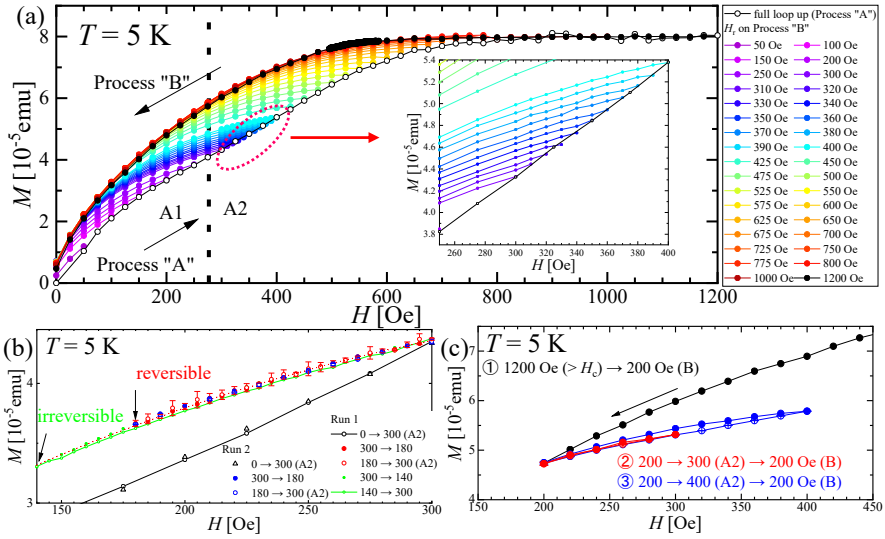

FIG. 3: (Color online) Full loop (FL) and single-return minor loop (SR-ML) M curves at 5 K. The open and solid circles represent the data for increasing and decreasing H, respectively. The inset shows SR-ML at intervals of 10 Oe for 300-400 Oe. (b) Double-return minor loop (DR-ML) magnetization curves from 300 Oe on A2 process at $T = 5$ K. The red dotted curve is guide for the eyes. (c) Double-return minor loop (DR-ML) magnetization curves from 200 Oe on B process at $T = 5$ K. In (b) and (c), the error bars are presented for the data for increasing H. In (c), the error bars are smaller than the symbol size.

N. DR-MLs showed the reversible changes whether they started from process A2 or B. Thus, the inside of the full loop can provide infinite states of N that depends on the H value apart from process A2 or process B.

To investigate the M-H curve at liquid helium temperature, use of the commercial SQUID magnetometer was necessary, which needs a certain minimum volume of crystal. Keeping S_{ab} at 0.55 mm × 0.30 mm, L_c was reduced to approximately 3 μm. Consequently, the hysteresis area of the full loop approached that obtained in the micro crystal for XMCD. The enlarged magnetic hysteresis observed in the process of changing H from 0 → 1200 ($> H_c$) → 0 indicates an enhancement of irreversibility between the soliton-annihilation and soliton-nucleation. This was achieved by modifying the crystal surface, i.e., the surface barrier for soliton penetration. The reduction of L_c also decreases the permittable soliton number, such that discreteness of M as a function of H should be enhanced. However, the stability of the discreteness is related to the geometrical factors of L_c, S_{ab}, surface flatness, and defects (dislocations or points defects).

At the initial stage of process A1, approximately half of the total solitons dissipate, and in process A2 covering 280-850 Oe, the residual approximately thirty solitons dissipate. Comaparing this situation as a clean system without a distribution of L_c and surface roughness, there must be a spatial distribution of N in the helical chain at each H. This means that N averaged for the entire crystal is not fixed to an integer value. The present accuracy of observing M is 4.7×10^{-7} emu. Referring to the previous mean-field theoretical results tells us that, in the present crystal with $L_c \sim 3$ μm, the change in M (ΔM) for $\Delta N = 1$ is approximately 1.3×10^{-6} emu, which is approximately three times the present accuracy [11, 23, 30]. Thus, in the present crystal, the actual controllability of locking N in the hysteresis of the full loop is much more than thirty patterns, and there is an infinite number of patterns for the N realized in the hysteresis area of the full M-H loop according to the experimental results.

We stabilized the magnetization curve of $CrNb_3S_6$ by reducing the size along helical axis of a single crystal to approximately 3 μm, enough to make the effects of the surface barrier prominent. First, we verified that the inside of full loop tracing between HM and FFM structures presents a region in which the soliton number is locked. By reducing the crystal size, the field range locking the soliton number was increased up to an interval with a level of 200 Oe level. Second, by utilizing non-negligible distribution (± 0.3 μm) of the thickness around 3 μm over large area, we created an infinite number of eigen states

in the inside of the hysteresis of the full loop, such that the possibility of application as a new memory device using the entire micro crystal (including the surface area) is promising.

We acknowledge Mr. K. Takahashi (Asahi International Techno Co. Ltd.) for the help in crystal machining. This work was supported by Grants-in-Aid for Scientific Research, Grant No. (S) 25220803, from the Ministry of Education, Culture, Sports, Science and Technology (MEXT), Japan. This work was also supported by the Center for Chiral Science in Hiroshima University (the MEXT program for promoting the enhancement of research universities, Japan) and JSPS Core-to-Core Program, A. Advanced Research Networks.

DATA AVAILABILITY

The data that support the findings of this study are available from the corresponding author upon reasonable request.

SUPPLEMENTARY MATERIAL

See supplementary material for measurements of the surface roughness by atomic force microscopy.

* Electronic address: m108022m@mail.kyutech.jp

[1] I. Dzyaloshinskii, J. Phys. Chem. Solid **4**, 241 (1958).
[2] T. Moriya, Phys. Rev. **120**, 91 (1960).
[3] Y. Togawa, T. Koyama, K. Takayanagi, S. Mori, Y. Kousaka, J. Akimitsu, S. Nishihara, K. Inoue, A. S. Ovchinnikov, and J. Kishine, Phys. Rev. Lett. **108**, 107202 (2012).
[4] S. Muhlbauer, B. Binz, F. Jonietz, C. Pfleiderer, A. Rosch, A. Neubauer, R. Georgii, and P. Boni, Science **323**, 915 (2009).
[5] X. Z. Yu, Y. Onose, N. Kanazawa, J. H. Park, J. H. Han, Y. Matsui, N. Nagaosa, and Y. Tokura, Nature **465**, 901 (2010).
[6] Y. Togawa, Y. Kousaka, K. Inoue, and J.-i. Kishine, J. Phys. Soc. Jpn. **85**, 112001 (2016).
[7] N. Nagaosa and Y. Tokura, Nature Nanotech **8**, 899 (2013).
[8] J.-i. Kishine, K. Inoue, and Y. Yoshida, Prog. Theor. Phys. Suppl. **159**, 82 (2005).
[9] I. Dzyaloshinskii, Sov. Phys. JETP **19**, 960 (1964).
[10] Y. A. Izyumov, Sov. Phys. Usp. **27**, 845 (1984).
[11] M. Mito, H. Ohsumi, K. Tsuruta, Y. Kotani, T. Nakamura, Y. Togawa, M. Shinozaki, Y. Kato, J.-i. Kishine, J.-i. Ohe, et al., Phys. Rev. B **97**, 024408 (2018).
[12] M. Shinozaki, Y. Masaki, R. Aoki, Y. Togawa, and Y. Kato, Phys. Rev. B **97**, 214413 (2018).
[13] M. N. Wilson, E. A. Karhu, D. P. Lake, A. S. Quigley, S. Meynell, A. N. Bogdanov, H. Fritzsche, U. K. Rößler, and T. L. Monchesky, Phys. Rev. B **88**, 214420 (2013).
[14] S. A. Meynell, M. N. Wilson, H. Fritzsche, A. N. Bogdanov, and T. L. Monchesky, Phys. Rev. B **90**, 014406 (2014).
[15] J. Müller, A. Rosch, and M. Garst, New J. Phys. **18**, 065006 (2016).
[16] A. O. Leonov and K. Inoue, Phys. Rev. B **98**, 054404 (2018).
[17] T. Miyadai, K. Kikuchi, H. Kondo, S. Sakka, M. Arai, and Y. Ishikawa, J. Phys. Soc. Jpn. **52**, 1394 (1983).
[18] Y. Kousaka, Y. Nakao, J. Kishine, M. Akita, K. Inoue, and J. Akimitsu, Nucl. Instrum. Methods Phys. Res., Sect. A **600**, 250 (2009).
[19] N. J. Ghimire, M. A. McGuire, D. S. Parker, B. Sipos, S. Tang, J.-Q. Yan, B. C. Sales, and D. Mandrus, Phys. Rev. B **87**, 104403 (2013).
[20] K. Tsuruta, M. Mito, Y. Kousaka, J. Akimitsu, J.-i. Kishine, Y. Togawa, H. Ohsumi, and K. Inoue, J. Phys. Soc. Jpn. **85**, 013707 (2016).
[21] K. Tsuruta, M. Mito, Y. Kousaka, J. Akimitsu, J. Kishine, Y. Togawa, and K. Inoue, Journal of Applied Physics **120**, 143901 (2016).
[22] K. Tsuruta, M. Mito, H. Deguchi, J. Kishine, Y. Kousaka, J. Akimitsu, and K. Inoue, Phys. Rev. B **93**, 104402 (2016).
[23] M. Ohkuma, M. Mito, N. Nakamura, K. Tsuruta, J. Ohe, M. Shinozaki, Y. Kato, J. Kishine, Y. Kousaka, J. Akimitsu, et al., AIP Advances **9**, 075212 (2019).
[24] Supplemental material.
[25] V. Laliena, J. Campo, J.-I. Kishine, A. S. Ovchinnikov, Y. Togawa, Y. Kousaka, and K. Inoue, Phys. Rev. B **93**, 134424 (2016).
[26] J.-i. Yonemura, Y. Shimamoto, T. Kida, D. Yoshizawa, Y. Kousaka, S. Nishihara, F. J. T. Goncalves, J. Akimitsu, K. Inoue, M. Hagiwara, et al., Phys. Rev. B **96**, 184423 (2017).
[27] M. Mito, S. Tominaga, Y. Komorida, H. Deguchi, S. Takagi, Y. Nakao, Y. Kousaka, and J. Akimitsu, J. Phys.: Conf. Ser. **215**, 012182 (2010).
[28] M. Mito, T. Tajiri, K. Tsuruta, H. Deguchi, J. Kishine, K. Inoue, Y. Kousaka, Y. Nakao, and J. Akimitsu, Journal of Applied Physics **117**, 183904 (2015).
[29] V. Dyadkin, F. Mushenok, A. Bosak, D. Menzel, S. Grigoriev, P. Pattison, and D. Chernyshov, Phys. Rev. B **91**, 184205 (2015).
[30] M. Shinozaki, S. Hoshino, Y. Masaki, J.-i. Kishine, and Y. Kato, J. Phys. Soc. Jpn. **85**, 074710 (2016).

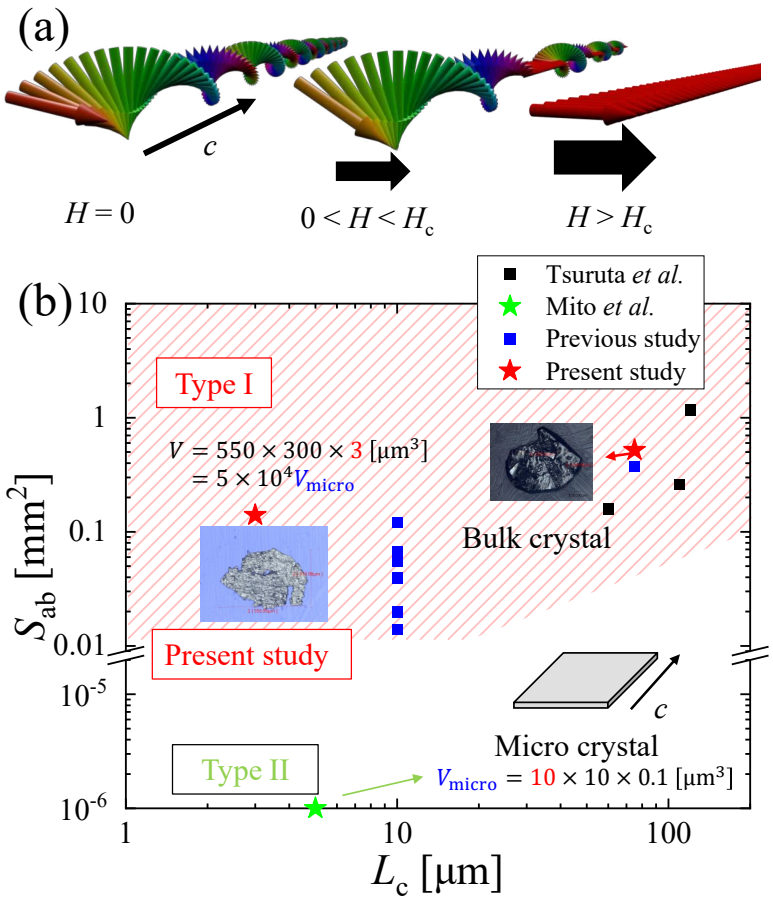

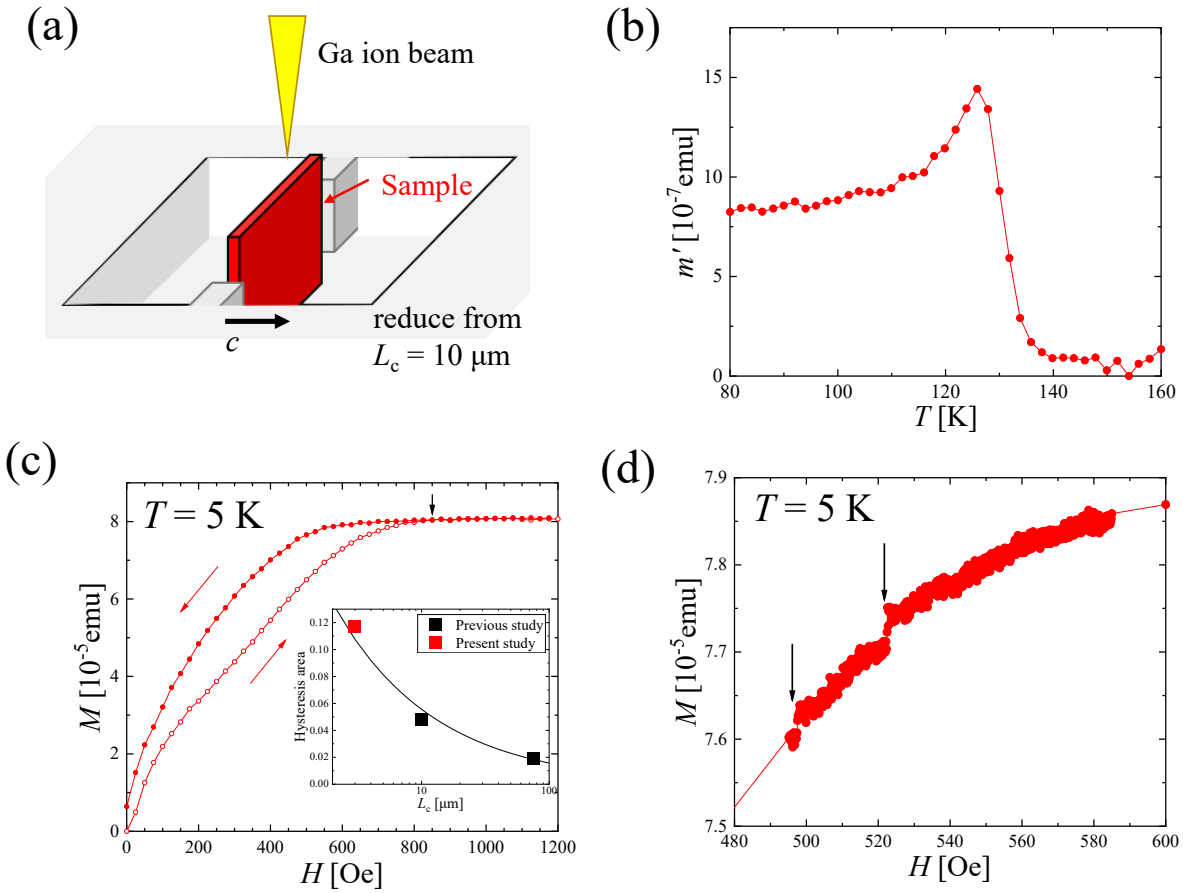

Applied Physics Letters